DOI: 10.1002/((please add manuscript number))

Article type: Communication

Engineering Ultrathin Polyaniline in Micro/Mesoporous Carbon Supercapacitor Electrodes using Oxidative Chemical Vapor Deposition

*Yuriy Y. Smolin, Katherine L. Van Aken, Muhammad Boota, Masoud Soroush, Yury Gogotsi, Kenneth K. S. Lau**

Y. Y. Smolin, Prof. M. Soroush, Prof. K. K. S. Lau

Department of Chemical and Biological Engineering, Drexel University, Philadelphia, PA 19104, USA. E-mail: klau@drexel.edu

K. L. Van Aken, M. Boota, Prof. Y. Gogotsi

Department of Materials Science and Engineering and A.J. Drexel Nanomaterials Institute, Drexel University. Philadelphia, PA 19104, USA.

Keywords: oxidative chemical vapor deposition, pseudocapacitance, supercapacitor, carbide-derived carbon, ultrathin polyaniline

Significant effort is currently being made to develop novel, environmentally friendly, inexpensive, and lightweight energy storage devices,[1] which are much in demand in a number of areas such as wearable electronics, automobiles, handheld devices, and power grids.[2-4] Compared to rechargeable batteries, supercapacitors have several advantages and a few disadvantages. They have higher power densities, are more environmentally friendly, but have lower energy densities. Their energy densities can be improved through integrating a pseudocapacitive material that stores charge via chemical reactions. Pseudocapacitive materials, such as intrinsically conducting polymers (ICPs) including polypyrrole, polythiophene, and polyaniline (PANI), are highly attractive because of their high theoretical gravimetric capacitance (400-750 F/g), sustainability, and relatively low cost.[5] By integrating ICPs within a carbon matrix, charge storage capacity can be improved significantly, since the reversible electrochemical reactions within ICPs store additional charge. The carbon matrix provides a conductive network for continuous ion percolation and the ICP offers high pseudocapacitance. However, supercapacitors utilizing ICPs exhibit poor cycle stability[5, 6] mainly due to thick polymer coatings, which swell and contract substantially on charge and discharge cycles, leading to mechanical degradation.[2] Another major drawback of the polymer integration is an uncontrolled formation of polymer aggregates during synthesis, which makes manufacturing of thin, uniform and conformal coatings difficult. Recently, advances have been made to integrate ICPs in supercapacitors to address these concerns by utilizing nanostructured polymer materials, via carbon-polymer composite devices such as polymer coatings onto carbon nanotubes (CNTs),[7] and by integrating ICPs directly onto conductive carbons, between graphene layers,[8] or between MXene layers.[9]

Current methods for coating polymers onto carbon substrates such as chemical bath deposition,[10] electrodeposition,[11] and casting from suspension[12] are unable to coat uniformly and conformally microporous (< 2 nm) carbon electrodes throughout the entire electrode thickness, typically 100 μm, without blocking pore accessibility to ions[2]. High pore aspect (length-to-width) ratio (>10,000), tortuous pore structure, liquid surface tension, solution viscosity, poor wettability, and solute steric hindrance make conformal coatings nearly impossible. Furthermore, poor solubility of ICPs in common solvents such as tetrahydrofuran, dimethylformamide, chloroform, and methanol, which is due to their rigid backbone structure, limits processability. Also, for electrochemical deposition, the need for a conductive substrate limits broad utility significantly. Overcoming these challenges can lead to substantially more use of ICPs in power storage. Ultrathin uniform conformal coating of microporous carbon electrodes can improve significantly the performance of ICP-integrated supercapacitors, since a highly-porous electrode with a 1-2 nm ultrathin uniform conformal polymer coating has several appealing features. First, it maintains the rapid movement of ions through the pores during charge/discharge reactions, preserving the electrochemical double layer capacitance (EDLC).[13] Second, due to the added faradaic redox reactions, the ICP coating can add pseudocapacitance charge storage. Third, the ICP in the nanometer-thin film will be accessible to the electrolyte and will be electrochemically active. These features improve the gravimetric and volumetric capacitance, and the energy density, because a 1-2 nm coating increases the device volume and mass very little.[3] Fourth, ultrathin coatings do not swell or contract significantly during cycling and are able to respond to stress better than thicker coatings, leading to better cyclability.[9] Fifth, thin films on conducting substrates can be used in high power applications, as they can undergo oxidation and reduction at very high rates.[2]

This work demonstrates that the current challenges in depositing ICPs onto porous carbon electrodes can be overcome and devices with improved electrochemical performance can be designed through oxidative chemical vapor deposition (oCVD). We deposit a 1-2 nm thin film of PANI onto carbide derived carbon (CDC) electrodes by oCVD, and then demonstrate improved device performance and excellent cyclability. To our knowledge, this is the first reported synthesis of PANI by oCVD. Mo_2C-CDC, which has a bimodal pore size distribution, is used to test the conformity and uniformity of polymer films because this material has a controlled pore size distribution in the nanometer range and a high specific surface area (SSA).[14] Due to its mix of micro-meso porosity, Mo_2C-CDC—as a model system—provides understanding of how the PANI film from oCVD coats different pore sizes and whether the size of the pore has an effect on the oCVD PANI integration.[15] CDCs are also advantageous in that their pore size can be tuned by adjusting synthesis temperature,[16] and as certain CDCs have multimodal pore size distributions, they are excellent for studying deposition of coatings into pores of different sizes.

oCVD is a simple, single step, solvent-free polymerization and coating technique, which has been shown to deposit conformal coatings thinner than 5 nm onto complex nanostructures,[17] flexible substrates, and within porous scaffolds.[18] oCVD polymerization mimics the oxidative step-growth polymerization that has been used widely to grow conducting polymers, where the combination of monomer and oxidant leads to a polymer thin film. oCVD involves surface polymerization, which facilitates conformal and uniform coatings.[19] The ability of oCVD to overcome the common challenges of solution deposition in solar cells has already been demonstrated.[7, 19, 20] Conducting polymer coatings of poly(3,4-ethylenedioxythiophene) (PEDOT), polythiophene (PT), and polypyrrole have been synthesized using oCVD.[19] Our previous use of

oCVD to create ultrathin coatings of PT showed that oCVD is able to deposit highly conformal and uniform coatings within porous nanostructures, such as anodized aluminum oxide, mesoporous titanium dioxide, and activated carbon.[17] The PT-coated activated carbon supercapacitor showed improved cyclability, with only a 10% decrease in capacitance after 5,000 cycles along with a 50% improvement in gravimetric capacitance, and a 250% increase in volumetric capacitance, compared to bare activated carbon.[17] The improvement was primarily due to the ultrathin coatings retaining the pore structure of the carbon, which maintained the EDLC, and incorporating simultaneously the redox reactions of the polymer provided additional charge storage and an increase in the double layer capacitance due to nanoconfinement.[17]

PANI is an ideal candidate for supercapacitors because it has many beneficial properties such as high electrical conductivity, high theoretical capacitance (55% higher than PT),[5] relatively low material cost, and greater stability than most other ICPs.[21] So, the successful integration of ultrathin PANI coatings into carbon materials can aid in overcoming current device limitations such as lower energy density of supercapacitors, compared to batteries. Furthermore, the PANI integration is relevant in many non-energy-related applications such as non-volatile memory and actuators, and benefits other fields such as membrane separations and catalysis. In this work, we are realizing the strategies proposed by Lukatskaya, Dunn, and Gogotsi[22] to improve both the energy and power densities of electrochemical capacitors by integrating PANI into a porous CDC electrode. As mentioned before, the oCVD deposition method provides better experimental control (e.g., coating thickness, polymer loading, etc.) for fabricating carbon/polyaniline devices[23, 24] than current solution-based methods. Moreover, oCVD is scalable to high throughput roll-to-roll processing for commercialization.

Figure 1 illustrates the oCVD process for PANI synthesis and integration. The aniline monomer and antimony pentachloride ($SbCl_5$) oxidant are vaporized and continuously fed into the reaction chamber. Nitrogen gas is used as an inert carrier to help transport the oxidant and as a diluent to control reaction kinetics. After entering the chamber, the oxidant and monomer diffuse into the pores of the carbon electrodes, adsorb onto the pore surfaces, and form PANI on CDC via an oxidative polymerization mechanism. After the film is deposited, it is washed with tetrahydrofuran (THF) to remove the oxidant.[17] Details of the experimental procedure are available in the Supporting Information.

Among ICPs, PANI is unique because it can exist in three different oxidation states. The fully oxidized pernigraniline state is composed fully of quinoid groups (N1 in **Figure 1**). At the other extreme, the fully reduced leucoemeraldine state is composed fully of benzenoid groups (N2 in **Figure 1**). In between, the partially oxidized emeraldine form is composed of a 1:1 ratio of benzenoid and quinoid groups. The emeraldine state is desired from an electrochemical standpoint, because its electrical conductivity is 10 orders of magnitude greater compared with the other two states.[25] Therefore, for electrochemical applications, it is essential to deposit emeraldine PANI via oCVD, and we use FTIR, XPS, and UV-vis to verify PANI formation. To quantify the formation of emeraldine PANI, FTIR analysis was performed on polymer films deposited onto silicon wafers via oCVD (**Figure 2a)**. Silicon wafers were selected because they are IR transparent. For FTIR, films of approximately 250 nm were analyzed, as determined by SEM, which also showed the films were dense and uniform (Supporting Information **Figure S1**). The lack of peaks at 749 and 688 cm^{-1} in the PANI spectrum indicates that the film is void of oligomers and short chain aniline units, more representative of the monomer (see Supporting Information for a detailed discussion of the aniline monomer peaks). In

addition, many of the peaks in the polymer spectrum indicate the formation of PANI. The peak around 1160 cm^{-1} is attributed to N=Q=N (Q=quinoid ring) and to aromatic C-H in-plane deformation, suggesting the formation of PANI.[26] A sharp peak at around 1148 cm^{-1} corresponds to $–NH^{+}=$ vibrations of PANI.[27] The peaks around 3000–3100 cm^{-1} are due to C–H stretching on the aromatic ring and NH_2^+ groups.[27] Furthermore, the band around 3304 cm^{-1} corresponds to free N–H symmetric stretching. Also, the peak at 825 cm^{-1} is consistent with high molecular weight PANI due to p-disubstitution and confirms para-coupling of the constitutive aniline units.[26, 28] The spectrum also indicate that the film is in the undoped state since the transition from undoped to doped states would blue shift the 825 and 1160 cm^{-1} peaks by 30 and 54 cm^{-1}, respectively.[29] The vibration around 1588 cm^{-1} represents the quinoid ring, and the 1510 cm^{-1} vibration is due to the benzenoid ring.[30] The presence of both 1510 and 1588 cm^{-1} peaks implies that both amine (N–C) and imine (N=C) units, respectively, exist within the polymer chains. Quantitatively, the ratio of the peak intensity at 1588 cm^{-1} to that at 1510 cm^{-1} has a value of 0.87, suggesting that most of the polymer is in the emeraldine form with slightly more benzenoid groups than quinoid groups.[31] This is supported by the peak at 1315 cm^{-1} which is due to C–H stretching of the secondary aromatic amine and suggests the formation of the emeraldine PANI.[26] The presence of emeraldine PANI is further supported by the green color of the PANI film, which is uniformly deposited via oCVD on a glass slide (**Figure 2b**).

UV-vis analysis (**Figure 2b**) indicates that the PANI film is in the undoped state, as suggested by the FTIR data. Doped PANI typically contains three absorption peaks located in the range of 306-324, 402-413, and 820-835 nm, corresponding to the benzenoid ring π-$π^*$, polaron-$π^*$, and π-polaron transitions, respectively.[28, 31, 32] The precise location of each peak depends on synthesis conditions

during deposition and the dopant used. In contrast, the oCVD PANI film contains only the two peaks centered around 314 and 434 nm. In general, the 820-835 nm peak provides a measure of the level of doping in the film and its absence indicates that the oxidant, antimony pentachloride, which also acts as the dopant, is not present in the oCVD PANI film, corroborating the FTIR results. This is attributed to the post-deposition washing step that removes the dopant, which has also been done previously for oCVD PEDOT and PT to improve performance.[19]

X-ray photoelectron spectroscopy (XPS) was used to investigate and quantify PANI film chemistry as well as to determine its oxidation state and doping level. As seen in **Figure 2c**, the N1s region can be resolved into three separate nitrogen bonding environments (corresponding to N1, N2, N3 in **Figure 1**). Previous XPS work on PANI[33, 34] have shown that N1 is the neutral imine nitrogen associated with the PANI quinoid groups, N2 is the neutral amine nitrogen in PANI benzenoid groups, and N3 is a more positively charged nitrogen group found in PANI. Also shown in **Figure 2c**, the C1s of oCVD PANI can likewise be resolved into three separate carbon environments. The lowest binding energy C1 peak corresponds to C–C and C–H bonds, the C2 peak corresponds to carbon bonded to neutral nitrogens such as N1 and N2, and the C3 peak corresponds to the C–N bond of N3. Since N1 and N2 correspond to quinoid and benzenoid groups, respectively, one can estimate the oxidation state by taking the ratio of the different nitrogen states: $(N1+N3)/N_{total}$.[34] For emeraldine PANI, this value should be 0.50. The oCVD PANI film has a ratio of 0.496, which suggests that most of the film is in the emeraldine state and provides more quantitative support of the FTIR analysis. The band positions and atomic percentage values for the fitted peaks, which validate the formation of emeraldine PANI, are summarized in **Table 1**.[33, 34] Based on the stoichiometry of the chemical structures shown in Figure 1, the ratio of C1 to (C2+C3) should be 2:1 for para coupling,

since C1 carbons are those not bonded to nitrogen. For oCVD PANI, the calculated ratio is smaller, at 1.72:1, primarily from a higher than expected C2 peak intensity compared to that predicted by the N1s XPS data and from theory. Based on previous work on polypyrrole and polyaniline, it has been proposed that hydrocarbon impurities on sample surfaces due to atmospheric exposure can affect the C–N bond intensity more than that of the C–C bond, which may account for the higher C2 value and lower C1/(C2+C3) ratio.[34, 35] Finally, the Cl2p and Sb5d signals indicate that 1.24 and 0.34 at% of chlorine and antimony, respectively, are present. This reflects a very low amount of antimony pentachloride left in the film after washing in THF, corroborating the UV-vis and FTIR analysis that washing removes nearly all the oxidant.

PANI was then deposited into Mo_2C-CDC electrodes and an asymmetric device was fabricated with an over-capacitive activated-carbon counter electrode, an Ag/AgCl reference electrode, and 1M H_2SO_4 as an electrolyte. The working electrode was either PANI-coated Mo_2C-CDC or uncoated Mo_2C-CDC. The performance of these supercapacitors was then compared. **Figure 3** shows the results of these tests, including a comparison of multiple scan rates for bare CDC (**Figure 3a**) and PANI-CDC (**Figure 3b**). **Figure 3a** depicts EDLC behavior of the bare CDC material, which is more resistive than other carbon materials due to the lower conductivity of the material. These performance values provide a baseline for measuring the improvement caused by the oCVD PANI coating. The gravimetric capacitance values of the bare CDC are between 70 to 17 F/g depending on scan rate. Different CDC materials have different electrochemical performances, and this baseline performance is evidence that Mo_2C-CDC as an electrode material is not as conductive as other porous materials. This is clear by the narrow shape of the CV curve for the bare CDC in aqueous electrolyte (**Figure 3a**). It also has a moderate SSA (530 m^2/g), hence showing a lower performance

compared to TiC-CDC.[14, 16, 36] From the second plot, there is a significant increase in the gravimetric capacitance of the PANI-coated CDC device (11 wt% of PANI in the CDC electrode), which varies between 155-115 F/g for scan rates between 5 and 500 mV/s. The oCVD PANI integrated supercapacitors have a specific capacitance more than twice that of bare CDC ones (136 F/g for 11 wt% of PANI in the CDC electrode vs. 60 F/g for bare CDC at 10 mV/s). This gives a PANI-only gravimetric capacitance of 690 F/g, very close to the theoretical limit of 750 F/g.[5] Further, the volumetric capacitance increased by 5.2 times (from 18 to 96 F/cm^3), assuming there is negligible increase in geometric volume with the ultrathin PANI coatings. The increase in capacitance is due to a faradaic redox reaction that occurs between PANI and protons,[37] causing a large increase in current and the peaks in the CV curve. Even at a high scan rate of 100 mV/s, the added pseudocapacitance from the PANI coating is still evident. **Figure 3c** shows the two devices at a single scan rate of 20 mV/s on a common capacitance scale. It provides a clearer comparison and again shows that the PANI coating not only adds a pseudocapacitive behavior to the device but also decreases the electrode resistance and increases the total capacitance, evidenced by the increase in the rectangular envelope compared to the bare CDC.

To gain a better understanding of the significant increase in gravimetric capacitance, and to understand what microscopic changes were taking place within the electrode due to the PANI coating, N_2 sorption measurements were done along with scanning electron microscopy (SEM). The surface area, pore size distribution, and pore volume were characterized by nitrogen sorption experiments, and the nitrogen adsorption-desorption isotherms (Supporting Information **Figure S2**) of both CDC and PANI-CDC films exhibited a type IV isotherm with a hysteresis, indicating micro-meso porosity. The hysteresis associated with PANI-CDC was slightly widened presumably as a result

of the PANI coating on CDC which may be due to a change in mesopore shape.[38] The CDC film exhibited a SSA of 530 m^2/g, which was reduced to 470 m^2/g after PANI coating. The slight decrease in SSA is most likely due to the PANI deposition, which coats and fills some pores. In contrast to solution-based approaches,[39] which typically decrease the surface area by 90%, oCVD coating decreased the SSA slightly, which is critical for charge storage applications and improving energy density without loss in power density. For instance, previous work on coating a pseudocapacitive material on graphene oxide sheets showed a decrease of SSA from 334 to 43 m^2/g.[40] Furthermore, pore widths of the PANI-CDC electrode were similar to the pristine CDC's pore widths of 0.81, 1.68 and 3.38 nm **(Figure 4a)**. Therefore, the pore geometry was retained during the coating process and the fabricated PANI-CDC film yielded high SSA, bimodal porosity, and open pore structure required for high charge storage capacitance. Also, the pore size distribution **(Figure 4a)** indicates that most PANI molecules were uniformly deposited in the pores, retaining the mixed porosity network for rapid charge/discharge and implying the coatings are extremely thin, on the order of a few nanometers or less based on TEM (Supporting Information **Figure S3**). To inspect the morphology of the coatings, top-down and cross-sectional SEM was performed on the samples. As seen in **Figure 4c**, PANI conformally coats the electrode and adds a unique porous morphology with pores between 5-50 nm in diameter that is not seen in the uncoated CDC (**Figure 4b**). In addition, it seems that some PANI was deposited on the surface of the electrode or between CDC grains, improving the electrical contacts between the grains and with the current collector. **Figure 4e** shows the cross-section of the film, which has an increased surface roughness within the electrode (**Figure 4e** inset) compared with bare CDC (**Figure 4d** and inset). Since the pore-size distribution was maintained, this underpins why the PANI-CDC device maintained a high capacitance. The PANI coating improved the

conductivity of the device (the pure carbon electrode was fairly resistive), leading to a more rectangular CV with greater capacitance. This may explain the increase in the CV envelope. As expected, this enhanced capacity is sensitive to PANI loading in the CDC electrodes (Supporting Information, **Figure S4**). For example, a CDC electrode fabricated with a lower PANI loading of 9 wt% (compared with 11 wt%) shows a similar increase in EDLC over bare CDC, attributed to the porous morphology, but a decrease in the redox peaks due to less PANI contributing to the faradaic pseudocapacitance. At a much higher PANI loading of 25 wt% (compared with 11 wt%), instead of increasing with loading, the sharp redox peaks decrease. This may be due to transport limitations that limit the full utilization of thicker PANI at higher loading. Previous work by our group on polythiophene-carbon supercapacitors has shown that there is an optimal polymer loading which provides the best synergy between faradaic redox reactions of the polymer and the double layer capacitance of the electrode.[17]

The effect of scan rate can be seen clearly in **Figure 3d**, where the performance of both devices decreases with scan rate. However, the PANI-coated electrode is notably better at retaining the capacitance, showing a shallower drop as the rate is increased, which can be due to the increased conductivity and the added redox capacitance, occurring at all rates caused by oCVD PANI. Electrochemical impedance spectroscopy results (Supporting Information **Figure S5**) validates that the resistance within the electrode was reduced by the oCVD PANI coating. This is very promising for high-power applications. The unique porous structure and ultrathin coating may facilitate the transport of ions throughout the electrode since thin polymer coatings were shown to perform very well in high power applications.[2] As shown through galvanostatic charge-discharge (Supporting Information, **Figure S6**), the CDC-PANI electrodes exhibit little IR drop and have good coulombic

efficiency. At a current density of 5, 10, and 50 A/g, the IR drop was 6.7, 13.3, and 66.9 mV, and the columbic efficiency was 77.8%, 73.5%, and 67.2%, respectively. The equivalent series resistance of the PANI-CDC was only 0.52 Ω. Finally, a typical disadvantage of PANI coating in electrochemical devices is significant degradation over cycling due to thick coatings swelling and contracting. Typically, conducting polymers begin to degrade under 1000 cycles due to changes in their physical structure that is caused by the repeated counter ion insertion and de-insertion causing changes in volume and mechanical failure.[5] For example, electrodeposited PANI on carbonized polyacrylonitrile aerogel electrodes lost 15.3% of the initial capacitance after only 200 cycles.[41] To examine the possible improvement of depositing oCVD PANI, the cycle life of both the bare and PANI-coated electrodes was tested over 10,000 cycles at a current density of 2 A/g (**Figure 3e)**. The bare CDC showed no change in capacitance over the 10,000 cycles, which was expected as traditional supercapacitor electrodes boast millions of cycles before failure[3]. This long cycle life is due to a physical adsorption mechanism that does not chemically modify the electrode. On the other hand, the PANI-coated electrodes revealed a higher capacitance due to the pseudocapacitive contribution of the PANI. In addition, after a minor drop in capacitance after the first few cycles, the performance of the PANI supercapacitor remains stable over the 10,000 cycles, dropping to only 90% of the initial stabilized value (~100 F/g). This suggests that the PANI coating is not only beneficial for boosting the overall capacitance, but can maintain this high capacitance over many charge-discharge cycles. Even after 10,000 cycles, the PANI-CDC device exhibited a 1.8 times greater capacitance than the bare CDC electrode.

In this work, we demonstrated that charge storage capacity of porous carbon can be improved significantly through the integration of nanometer-thin PANI films into CDC electrodes

with a bimodal (micro/mesoporous) pore size distribution using the single-step oCVD process. To our knowledge, this work is the first reported synthesis of PANI via oCVD on different substrates. The oCVD process allows for the integration of PANI into pores as small as 1.7 nm, and CDC/PANI electrodes have a gravimetric capacitance more than twice that of bare CDC (136 F/g for 11 wt% of PANI in the CDC electrode vs. 60 F/g for bare Mo_2C-CDC at 10 mV/s). This yields a PANI-only gravimetric capacitance of ~690 F/g, which is close to the theoretical value of 750 F/g.[5] The coating preserves to a large extent the native electrode surface area and pore size distribution, while simultaneously improving capacitance due to the faradaic redox reactions of PANI. Even at high scan rates of over 100 mV/s, the added pseudocapacitance from PANI remained evident. The composite electrode exhibited good cyclability, decreasing to 90% of the initially value (~100 F/g) after 10,000 cycles. The remarkable improvements in electrochemical performance can be attributed to the major advantages of using oCVD, which provides much finer control over film properties and thickness. This aids in fabricating supercapacitors with ultrathin PANI coatings at small PANI loading that are more robust, which is extremely challenging using conventional solution-based methods. For instance, work by Cong et al., reported that, while a bare graphene paper electrode was ~30 µm, the graphene paper electrode electropolymerized with PANI was 38 µm, and the thick PANI coating contributed to the 18% drop in capacitance after 1000 cycles (at 5 A/g and 22.3 wt % PANI).[42] Likewise, Wu et al., has shown that 120 nm diameter PANI nanofibers synthesized by interfacial polymerization and integrated into graphene layers exhibited a 21% drop in capacitance after 800 cycles (at 3 A/g and 66% wt% PANI)[24]. Furthermore, composites of single-walled carbon nanotubes and 50 nm thick chemically polymerized PANI nanoribbons showed a 21% reduction in capacitance after 1000 cycles (at 0.2 mA/cm^2 and 26 wt% PANI).[43] Similarly, carbon nanocoils (80-100 nm

diameter) integrated with chemically polymerized PANI (80 wt %, 20 nm thick) exhibited a 28% drop in capacitance after 2000 cycles (at 2.5 A/g).[44] In addition to the poor cyclability, most of the solution-based composite devices only reach PANI-only capacitances that are ~60–70% of the theoretical limit. In contrast, the oCVD process enables nanometer-thin control of PANI coatings which, with the smaller PANI loadings, leads to excellent cyclability even after 10,000 cycles, show very good rate performance, and have PANI-only capacities up to 92% of the theoretical limit.

Supporting Information

Supporting Information is available from the Wiley Online Library or from the author.

Acknowledgements

K. K. S. Lau, M. Soroush, and Y. Y. Smolin acknowledge support from the National Science Foundation, Grant No. CBET-1236180. K. K. S. Lau further acknowledges support from NSF CBET-1264487. K. L. Van. Aken, M. Boota, and Y. Gogotsi acknowledge support from the Fluid Interface Reactions, Structures, and Transport (FIRST) Center, an Energy Frontier Research Center funded by the U.S. Department of Energy, Office of Science, Office of Basic Energy Sciences. The authors would also like to acknowledge the use of Drexel University's Core Facilities, and the assistance from Seyong Kim and Yawei Li with TEM imaging.

Received: ((will be filled in by the editorial staff))
Revised: ((will be filled in by the editorial staff))
Published online: ((will be filled in by the editorial staff))

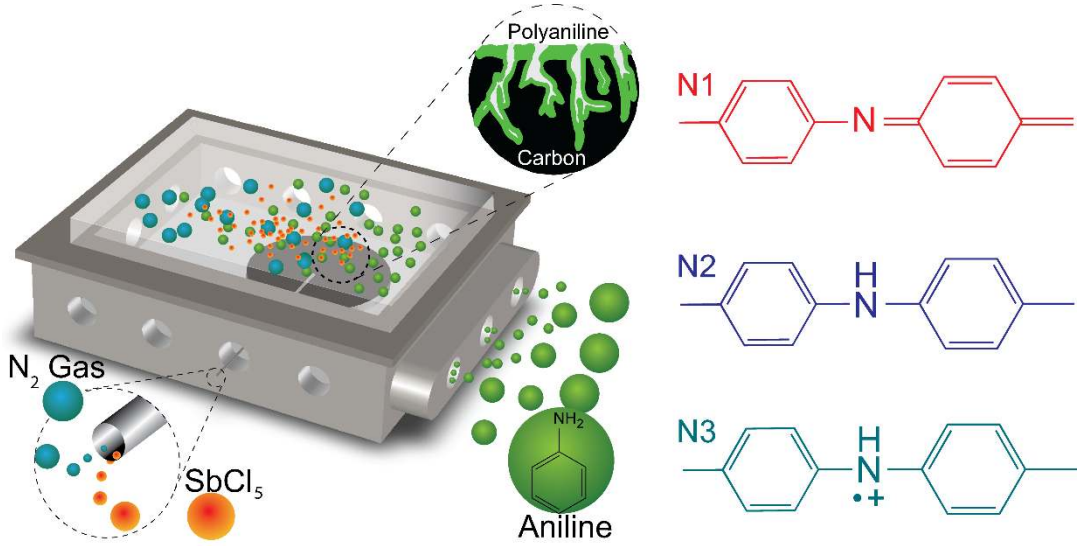

Figure 1. (left) Synthesis and integration of PANI in carbon supercapacitor electrodes by oCVD. oCVD enables polymerization and conformal thin film formation of PANI onto a porous carbon electrode. (right) Chemical structure of different states of PANI.

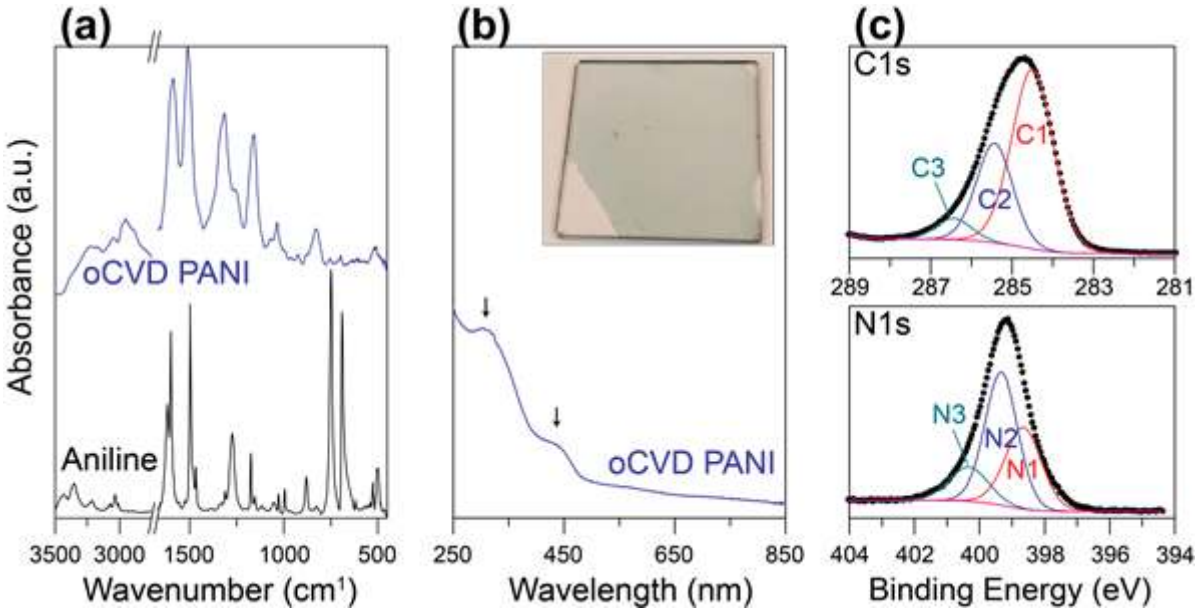

Figure 2. (a) FTIR of aniline monomer (bottom) and oCVD PANI thin film (top). (b) UV-vis absorption spectrum of oCVD PANI film. Inset: PANI, deposited onto quartz glass, shows a green color indicative of the emeraldine state. (c) High resolution N1s and C1s XPS spectra of oCVD PANI thin films corresponding to chemical groups in Fig.1.

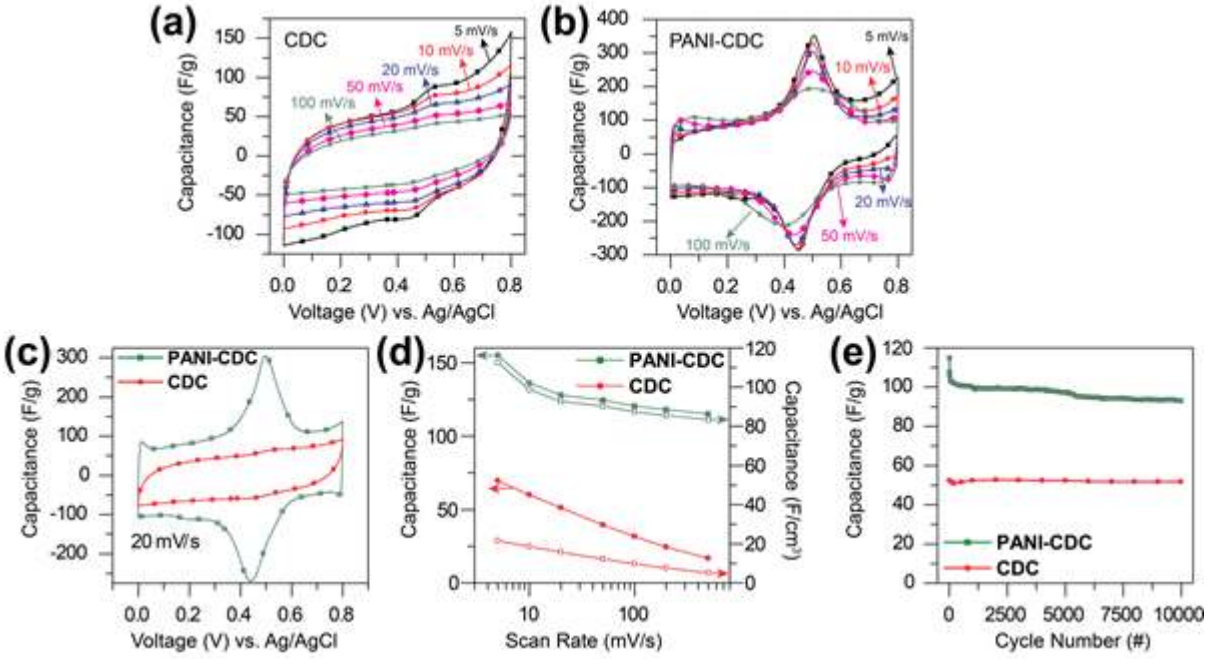

Figure 3. Cyclic voltammograms in a range of scan rates for (a) bare, and (b) PANI-coated Mo_2C-CDC electrodes. (c) A common-scale comparison of the cyclic voltammograms for both electrodes at 20 mV/s, where the PANI-coated electrode (green square) shows a pseudocapacitive contribution as well as an increase in EDL capacitance compared to the bare Mo_2C-CDC (red circle). (d) Rate performance, in terms of specific (closed symbols) and volumetric (open symbols) capacitance of both devices, calculated from the cyclic voltammograms shown in (a) and (b). (e) Cycle life of each device, tested at 20 mV/s for 10,000 cycles.

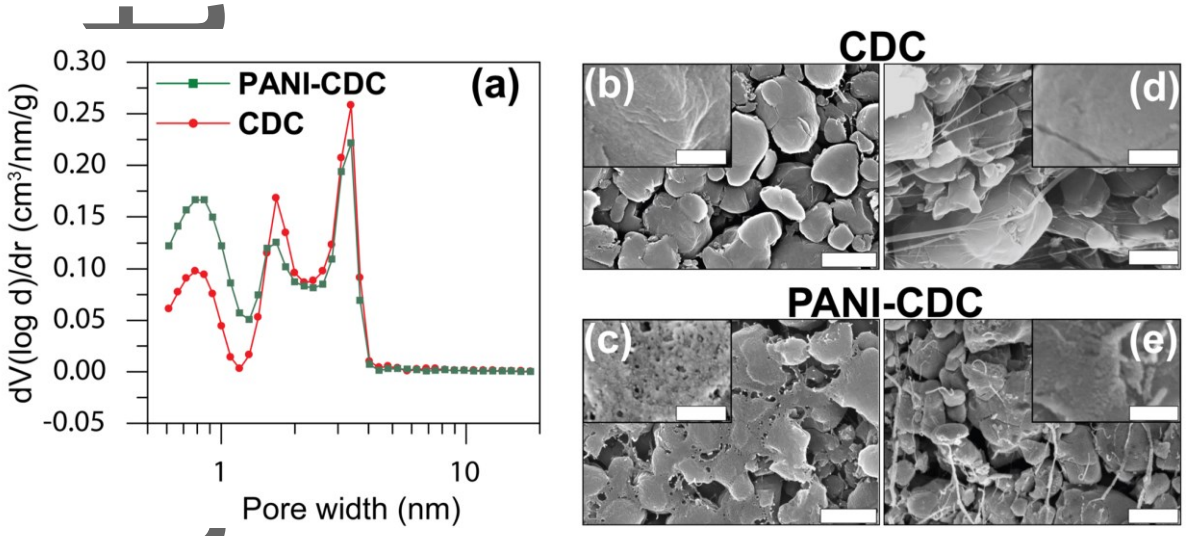

Figure 4. (a) Pore size distributions of bare (red circle) and PANI-coated Mo_2C-CDC (green square) electrodes. (b, c) Top-down SEM images of bare and PANI-coated Mo_2C-CDC electrodes, respectively. (d, e) Cross-sectional SEM images of bare and PANI-coated Mo_2C-CDC electrodes, respectively. Scale bar: 2 µm, inset: 400 nm.

Table 1. Resolved peak data from the N1s and C1s XPS spectra.

	N1	N2	N3	C1	C2	C3
Energy (eV)	398.7	399.3	400.4	284.5	285.3	286.0
Atomic %	34.2	50.4	15.4	63.2	30.5	6.3

Novel oxidative chemical vapor deposition (oCVD) synthesis and integration of ultrathin polyaniline into micro/mesoporous carbide derived carbon (Mo_2C-CDC) supercapacitor electrodes. A combination of spectroscopic techniques confirmed that the oCVD process produces electrochemically active emeraldine PANI. The composite electrode exhibited a two times improvement in specific capacitance vs bare Mo_2C-CDC and showed good cyclability.

Keywords: oxidative chemical vapor deposition, pseudocapacitance, supercapacitor, carbide-derived carbon, polyaniline

Yuriy Y. Smolin, Katherine L. Van Aken, Muhammad Boota, Masoud Soroush, Yury Gogotsi, Kenneth K. S. Lau

Engineering Ultrathin Polyaniline in Micro/mesoporous Carbon Supercapacitor Electrodes using Oxidative Chemical Vapor Deposition

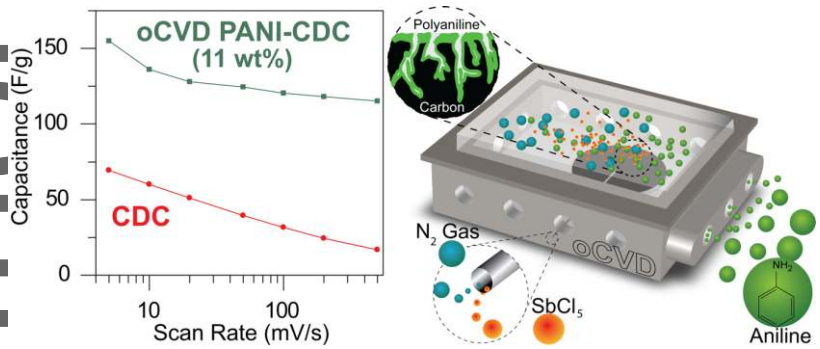

References

[1] S. Muench, A. Wild, C. Friebe, B. Häupler, T. Janoschka, U. S. Schubert, Chemical Reviews 2016, 116, 9438; Y. Shao, M. F. El-Kady, L. J. Wang, Q. Zhang, Y. Li, H. Wang, M. F. Mousavi, R. B. Kaner, *Chem. Soc. Rev.* **2015**, *44*, 3639.

[2] L. Nyholm, G. Nyström, A. Mihranyan, M. Strømme, *Adv. Mater.* **2011**, *23*, 3751.

[3] P. Simon, Y. Gogotsi, *Nat. Mater.* **2008**, *7*, 845.

[4] K. T. Nam, D.-W. Kim, P. J. Yoo, C.-Y. Chiang, N. Meethong, P. T. Hammond, Y.-M. Chiang, A. M. Belcher, *Science* **2006**, *312*, 885; H. Nishide, K. Oyaizu, *Science* **2008**, *319*, 737.

[5] G. A. Snook, P. Kao, A. S. Best, *J. Power Sources* **2011**, *196*, 1.

[6] P. Novák, K. Müller, K. S. V. Santhanam, O. Haas, *Chem. Rev.* **1997**, *97*, 207; K. Naoi M. Morita, *Electrochem. Soc. Interface* **2008**, *17*, 44; K. Naoi, P. Simon, *J. Electrochem. Soc.* **2008**, *17*, 34.

[7] Y. Zhou, N. Lachman, M. Ghaffari, H. Xu, D. Bhattacharya, P. Fattahi, M. R. Abidian, S. Wu, K. K. Gleason, B. L. Wardle, Q. M. Zhang, *J. Mater. Chem. A* **2014**, *2*, 9964.

[8] Y. Zhao, J. Liu, Y. Hu, H. Cheng, C. Hu, C. Jiang, L. Jiang, A. Cao, L. Qu, *Adv. Mater.* **2013**, *25*, 591.

[9] M. Boota, B. Anasori, C. Voigt, M.-Q. Zhao, M. W. Barsoum, Y. Gogotsi, *Adv. Mater.* **2016**, *28*, 1517.

[10] W.-S. Huang, B. D. Humphrey, A. G. MacDiarmid, *J. Chem. Soc., Faraday Trans. 1* **1986**, *82*, 2385.

[11] G. Zotti, S. Cattarin, N. Comisso, *J. Electroanal. Chem.* **1987**, *235*, 259.

[12] A. Andreatta, Y. Cao, J. C. Chiang, A. J. Heeger, P. Smith, *Synth. Met.* **1988**, *26*, 383.

[13] M. Boota, K. B. Hatzell, E. C. Kumbur, Y. Gogotsi, *ChemSusChem* **2015**, *8*, 835; M. Boota, M. P. Paranthaman, A. K. Naskar, Y. Li, K. Akato, Y. Gogotsi, *ChemSusChem* **2015**, *8*, 3576.

[14] H. S. Kim, J. P. Singer, Y. Gogotsi, J. E. Fischer, *Microporous Mesoporous Mater.* **2009**, *120*, 267.

[15] V. Presser, M. Heon, Y. Gogotsi, *Adv. Funct. Mater.* **2011**, *21*, 810.

[16] G. Laudisio, R. K. Dash, J. P. Singer, G. Yushin, Y. Gogotsi, J. E. Fischer, *Langmuir* **2006**, *22*, 8945.

[17] S. Nejati, T. E. Minford, Y. Y. Smolin, K. K. S. Lau, *ACS Nano* **2014**, *8*, 5413.

[18] W. E. Tenhaeff, K. K. Gleason, *Adv. Funct. Mater.* **2008**, *18*, 979; S. H. Baxamusa, S. G. Im, K. K. Gleason, *Phys. Chem. Chem. Phys.* **2009**, *11*, 5227; Trujillo, N.J., Barr, M.C., Im, S.G., Gleason, K. K., *J. Mater. Chem.* **2010**, *20*, 3968.

[19] K. K. Gleason, *CVD Polymers: Fabrication of Organic Surfaces and Devices*, John Wiley & Sons, 2015.

[20] Y. Y. Smolin, S. Nejati, M. Bavarian, D. Lee, K. K. S. Lau, M. Soroush, *J. Power Sources* **2015**, *274*, 156.

[21] S. Bhadra, D. Khastgir, N. K. Singha, J. H. Lee, *Prog. Polym. Sci.* **2009**, *34*, 783.

[22] M. R. Lukatskaya, B. Dunn, Y. Gogotsi, *Nat. Commun.* **2016**, *7*, 12647.

[23] D.-W. Wang, F. Li, J. Zhao, W. Ren, Z.-G. Chen, J. Tan, Z.-S. Wu, I. Gentle, G. Q. Lu, H.-M. Cheng, *ACS Nano* **2009**, *3*, 1745.

[24] Q. Wu, Y. Xu, Z. Yao, A. Liu, G. Shi, *ACS Nano* **2010**, *4*, 1963.

[25] J.-C. Chiang, A. G. MacDiarmid, *Synth. Met.* **1986**, *13*, 193.

[26] J. Stejskal, M. Trchová, *Polym. Int.* **2012,** *61*, 240.

[27] I. Šeděnková, M. Trchová, N. V. Blinova, J. Stejskal, *Thin Solid Films* **2006**, *515*, 1640.

[28] G. A. Zaharias, H. H. Shi, S. F. Bent, *Thin Solid Films* **2006**, *501*, 341.

[29] J. Li, X. Tang, H. Li, Y. Yan, Q. Zhang, *Synth. Met.* **2010**, *160*, 1153.

[30] L.-M. Huang, T.-C. Wen, A. Gopalan, *Mater. Lett.* **2003**, *57*, 1765.

[31] T. Abdiryim, Z. Xiao-Gang, R. Jamal, *Mater. Chem. Phys.* **2005**, *90*, 367.

[32] W. Wang, A. G. MacDiarmid, *Synth. Met.* **2002**, *129*, 199; A. Gruger, A. Novak, A. Régis, P. Colomban, *J. Mol. Struct.* **1994**, *328*, 153; M. Alam, A. A. Ansari, M. R. Shaik, N. M. Alandis, *Arab. J. Chem.* **2013**, *6*, 341.

[33] K. L. Tan, B. T. G. Tan, E. T. Kang, K. G. Neoh, *Phys. Rev. B* **1989**, *39*, 8070; S. Golczak, A. Kanciurzewska, M. Fahlman, K. Langer, J. J. Langer, *Solid State Ionics* **2008**, *179*, 2234; X.-R. Zeng, T.-M. Ko, *Polymer* **1998**, *39*, 1187; S. N. Kumar, F. Gaillard, G. Bouyssoux, A. Sartre, *Synth. Met.* **1990**, *36*, 111.

[34] S. N. Kumar, G. Bouyssoux, F. Gaillard, *Surf. Interface Anal.* **1990**, *15*, 531.

[35] P. Pfluger, G. B. Street, *J. Chem. Phys.* **1984**, *80*, 544.

[36] Y. Gao, V. Presser, L. Zhang, J. J. Niu, J. K. McDonough, C. R. Pérez, H. Lin, H. Fong, Y. Gogotsi, *J. Power Sources* **2012**, *201*, 368.

[37] P. Sekar, B. Anothumakkool, V. Vijayakumar, A. Lohgaonkar, S. Kurungot, *ChemElectroChem* **2016**, *3*, 933.

[38] E. N. Hoffman, G. Yushin, M. W. Barsoum, Y. Gogotsi, *Chem. Mater.* **2005**, *17*, 2317.

[39] L. Li, H. Song, Q. Zhang, J. Yao, X. Chen, *J. Power Sources* **2009**, *187*, 268.

[40] M. Boota, C. Chen, M. Becuwe, L. Miao, Y. Gogotsi, *Energy Environ. Sci.* **2016**, *9*, 2586.

[41] H. Talbi, P.-E. Just, L. Dao, *J. Appl. Electrochem.* **2003**, *33*, 465.

[42] H.-P. Cong, X.-C. Ren, P. Wang, S.-H. Yu, *Energy & Envir. Sci.* **2013**, *6*, 1185.

[43] D. Ge, L. Yang, L. Fan, C. Zhang, X. Xiao, Y. Gogotsi, S. Yang, *Nano Energy* **2015**, *11*, 568.

[44] R. B. Rakhi, W. Chen, H. N. Alshareef, *J. Mat. Chem.* **2012**, *22*, 5177.